International Journal of Greenhouse Gas Control 23 (2014) 113–118

Contents lists available at ScienceDirect

International Journal of Greenhouse Gas Control

journal homepage: www.elsevier.com/locate/ijggc

Theoretical analysis of how pressure buildup and CO_2 migration can both constrain storage capacity in deep saline aquifers

M.L. Szulczewski, C.W. MacMinn [1], R. Juanes *

Massachusetts Institute of Technology, 77 Massachusetts Avenue, Cambridge, MA, USA

ARTICLE INFO

Article history:
Received 26 January 2013
Received in revised form 12 February 2014
Accepted 17 February 2014

Keywords:
Carbon dioxide sequestration
Deep saline aquifers
Storage capacity
Overpressure
Residual trapping
Analytical models

ABSTRACT

Estimating the carbon dioxide (CO_2) storage capacity of deep saline aquifers is important for identifying those most suitable for sequestration, and for planning the future development of CO_2 storage projects. Currently, capacity estimates are highly uncertain due in part to uncertainty in the dominant constraint on capacity: both the pressure buildup from injection and the space available to trap CO_2 have been identified as constraints, but have not been rigorously compared to determine the conditions under which each is more limiting. In this study, we evaluate their relative importance in an idealized aquifer using simple, but dynamic models of how pressure rises during injection and how CO_2 becomes trapped in the pore space. We show that there exists a crossover injection duration, T_c, below which pressure constraints dominate, but above which the CO_2 migration becomes the more limiting constraint. We illustrate this behavior by applying the models to the Fox Hills Sandstone.

1. Introduction

Capturing CO_2 from power plants and storing it in underground reservoirs can help abate anthropogenic CO_2 emissions from burning fossil fuels (MIT, 2007; Scott et al., 2013; Rogelj et al., 2013). Some of the most promising storage reservoirs are deep saline aquifers, which are layers of sandstone or carbonate located several kilometers underground and saturated with saline water (Lackner, 2003). They are attractive places to sequester CO_2 because they are widespread and their water is typically too saline for drinking or agriculture (Orr, 2009).

An important measure of the suitability of a deep saline aquifer for storage is how much CO_2 it can hold, called its storage capacity (Bachu et al., 2007; Bradshaw et al., 2007). One way to calculate it is based on the pore volume of an aquifer and how the injected CO_2 would occupy it. For example, in the Carbon Sequestration Atlas of the United States, storage capacity is calculated as the total free-phase CO_2 that would occupy the pore space of an aquifer, accounting for factors such as heterogeneity, residual water, and sweep efficiency (National Energy Technology Laboratory, 2010). In Dooley et al. (2004), it is calculated as the total CO_2 that could be dissolved in all the water in the pore space. We refer to these types of capacities as volume limited.

While some studies use volumetric constraints, others use pressure constraints (Zhou et al., 2008; Ehlig-Economides and Economides, 2010). These studies calculate the storage capacity as the maximum amount of CO_2 that can be injected before the increase in pressure causes fractures or activates faults. Fracturing and fault activation could induce seismicity, or could create or enhance pathways by which CO_2 could leak from the target aquifer (IPCC, 2005; Cappa and Rutqvist, 2011a,b; Morris et al., 2011). We refer to storage capacities based on this type of constraint as pressure limited.

One shortcoming of all of these methods to calculate capacity is that they are based on a single constraint—either pressure or pore volume. Since the most limiting constraint is unknown *a priori*, the appropriate method to use is unclear *a priori*.

In a previous paper, we used numerical simulations and found that the dominant constraint depends on the aquifer properties and the properties of the injection scenario (Szulczewski et al., 2012). Here, we consider a simpler system to develop analytical expressions that clarify how different properties of the aquifer and injection scenario affect the dominant constraint. The system is a homogeneous, isotropic aquifer at the scale of an entire geologic basin (Fig. 1). We consider this scale because large quantities of CO_2 (100s of millions of metric tons) will have to be stored to significantly reduce emissions. CO_2 is injected into the aquifer from a line-drive array of wells, in which the wells are close enough that

* Corresponding author. Tel.: +1 6172537191.
E-mail address: juanes@mit.edu (R. Juanes).
[1] Present address: Oxford University, Oxford, UK.

http://dx.doi.org/10.1016/j.ijggc.2014.02.006
1750-5836/

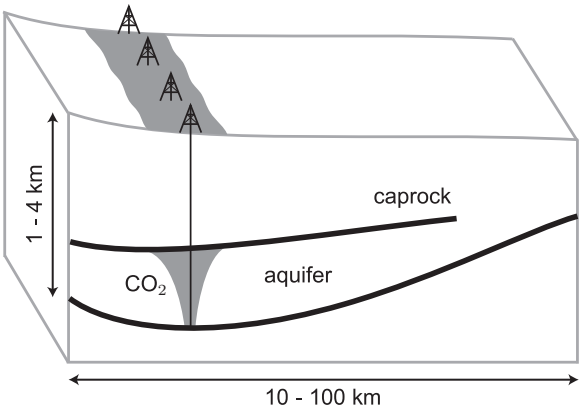

Fig. 1. We compare pressure and migration constraints on storage capacity in a model system: a deep saline aquifer at the basin scale, into which CO_2 is injected from a line-drive array of wells.

the pressure and CO_2 distribution along the line drive becomes nearly uniform shortly after injection begins (Nicot, 2008). This well geometry allows us to collapse the dimension along the line drive and model the system in a cross section through the aquifer. While the exact configuration and number of injection wells will ultimately be impacted by economics, politics, and legal factors (Dooley, 2011; Bachu et al., 2007), we neglect these issues to focus on the physics of injection and trapping. After injection, CO_2 migrates upslope or in the direction of the natural groundwater through-flow (Juanes et al., 2010; MacMinn et al., 2010).

To evaluate pressure and volumetric constraints in this system, we develop models for the pressure-limited and migration-limited storage capacities. Since the smaller capacity comes from the more limiting constraint, we compare the size of the capacities to evaluate the relative severity of the constraints. While the capacity models are based on many simplifications, we expect results that are at least of the correct order of magnitude, which are sufficient to delineate the general conditions under which pressure or migration is the more limiting constraint. Although we do not undertake them here, the estimates of storage capacity are amenable to sensitivity and uncertainty analyses (Szulczewski et al., 2012).

2. Migration-limited capacity

We calculate the migration-limited capacity as the mass of CO_2 that can be trapped in an aquifer due to residual trapping. In residual trapping, CO_2 is trapped by capillary forces whenever it is displaced by brine, as at the trailing edge of a plume of migrating CO_2 (Fig. 2) (Juanes et al., 2006). We neglect CO_2 that may be trapped in carbonate minerals because mineral trapping occurs over timescales that are much longer than those associated with residual trapping (IPCC, 2005). For simplicity, we also neglect CO_2 that may be trapped via dissolution into the brine, although this can be an important contribution to the overall storage capacity (Gasda et al., 2011; MacMinn et al., 2011).

The total mass of CO_2 trapped by residual trapping is controlled by two factors: the fraction of total aquifer volume that is swept by CO_2, and the fraction of CO_2 that is trapped in the swept volume. The first factor is controlled by how CO_2 migrates in the aquifer. Since it is buoyant and less viscous than brine, the CO_2 will preferentially travel in a long, thin tongue along the caprock (Hesse et al., 2008). This causes residual trapping to occur in only a small fraction of the available pore space (Fig. 2). The second factor is a function of the porosity and the residual gas saturation.

To calculate the mass of residual CO_2, we use a simple but dynamic model for how CO_2 migrates in an aquifer. The model is a hyperbolic partial differential equation, and has been derived in previous papers (Juanes et al., 2010; MacMinn et al., 2010; Szulczewski et al., 2012). It is based on the following assumptions:

1. The interface between the CO_2 and brine is sharp (sharp-interface approximation) (Bear, 1972).
2. Capillary pressure is negligible compared to typical viscous pressure drops and hydrostatic pressure drops.
3. Vertical flow velocities are negligible compared to lateral flow velocities (vertical-flow equilibrium, or the Dupuit approximation) (Bear, 1972; Yortsos, 1995).
4. The fluids are incompressible and Newtonian.
5. Fluid properties are uniform and constant.
6. The aquifer is rigid, homogeneous and isotropic.

For the case in which CO_2 migration is driven solely by the natural hydraulic gradient in the aquifer, the fraction of aquifer volume occupied by residual CO_2, ε_f, is (Juanes et al., 2010):

$$\varepsilon_f = \frac{V_g}{WHL_g} = \frac{\Gamma}{(1-(\Gamma/2)(1-\Gamma))M-(1-(\Gamma/2))(1-\Gamma)}, \tag{1}$$

where W is the width of the well array, H is the aquifer thickness, and L_g is the lateral extent of aquifer swept by CO_2 at the point when it becomes fully trapped (measured perpendicular to the well array). Therefore, WHL_g is the volume of a box which just encloses the plume of trapped CO_2. The volume of aquifer actually occupied by trapped CO_2 is V_g, which includes the volume of the rock and connate water. Here, Γ is the trapping coefficient: the ratio of the pore volume occupied by residual CO_2 to the pore volume initially occupied by CO_2, $\Gamma = S_{gr}/(1-S_{wc})$, where S_{gr} is the residual CO_2 saturation and S_{wc} is the connate water saturation. M is the ratio of the mobility of CO_2 to the mobility of brine: $M = \mu_w k^*_{rg}/\mu_g$, where μ_w is the viscosity of brine, μ_g is the viscosity of CO_2, and k^*_{rg} is the endpoint relative permeability to CO_2 (Oak et al., 1990; Bennion and Bachu, 2008). For the case in which only buoyancy drives migration of the CO_2 upslope, the volume fraction of an aquifer containing residual CO_2 is given to a good approximation by (MacMinn et al., 2010):

$$\varepsilon_s = \frac{V_g}{WHL_g} = \frac{\Gamma}{0.9M+0.49}. \tag{2}$$

These fractions are typically called efficiency factors (Bachu et al., 2007; Juanes et al., 2010).

With the efficiency factor, we calculate the storage capacity in three steps. First, we rearrange the expression for the efficiency factor to solve for the volume of aquifer occupied by trapped CO_2, V_g. Next, we require that the lateral extent of the trapped CO_2, L_g, exactly equals the lateral extent of the aquifer that is suitable for CO_2 storage, L, which must be interpreted from the hydrogeology (Section 5). This stipulation ensures that the trapped plume fits exactly inside the aquifer. Finally, we convert the volume of aquifer occupied by CO_2 to the mass of CO_2 in the pores by multiplying by the porosity, ϕ, the residual gas saturation, S_{gr}, and the CO_2 density, ρ_g. The resulting equation for the migration-limited storage capacity is:

$$C_m = LHW\rho_g\phi S_{gr}\varepsilon. \tag{3}$$

3. Pressure-limited capacity

We calculate the pressure-limited capacity to be the total amount of CO_2 that can be injected before the pressure rise creates a tensile fracture in the caprock. While shear failure may occur first, we choose tensile fracturing as the constraint for simplicity: predicting tensile fracturing requires only the minimum

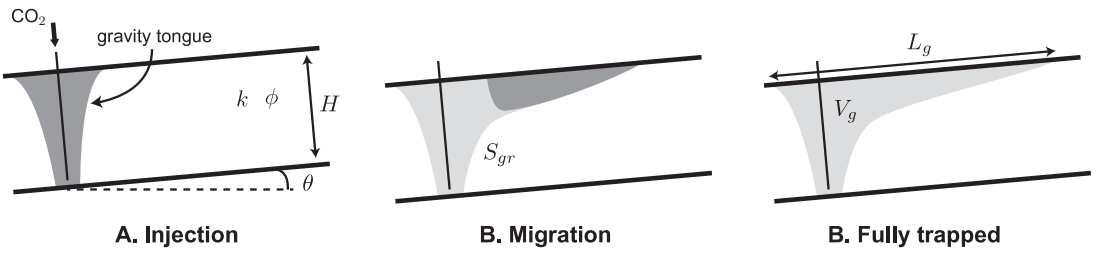

Fig. 2. To calculate the migration-limited capacity, we model how CO_2 migrates in an aquifer. (A) During injection, the CO_2 migrates nearly symmetrically away from the well array. It begins forming a gravity tongue because it is much less viscous than the brine. (B) After injection has stopped, the CO_2 migrates upslope due to buoyancy or downstream due to groundwater flow in a more exacerbated gravity tongue. It becomes trapped at the trailing edge of the plume at saturation S_{gr} (light gray area). (C) Eventually the plume becomes completely trapped, reaching a lateral extent L_g and filling a fraction of the aquifer volume V_g. By requiring that the plume extent equal the aquifer extent, L, we can calculate the total amount of CO_2 that can be injected such that the trapped plume fits exactly inside the reservoir.

principal effective stress in the aquifer, while predicting shear failure requires the entire stress tensor, which is often unavailable in practice (Zoback, 2007).

To calculate the pressure that would cause fracturing, we use the effective stress principle:

$$\sigma' = \sigma - bp, \tag{4}$$

where σ' is the effective stress, σ is the total stress, p is the pore pressure, and b is the Biot poroelastic coefficient, which we take to be one. Ignoring the cohesive strength of the aquifer, which is often negligible in practice (Zoback, 2007, p.121), a tensile fracture occurs when the minimum principal effective stress is zero. This indicates that the fracture pressure equals the minimum principal total stress: $p_{\text{frac}} = \sigma_3$. When this stress is vertical, we calculate it to be the weight of the overburden:

$$p_{\text{frac}} = (1-\phi)\rho_r g D + \phi \rho_w g D, \tag{5}$$

where D is the depth to the top of the aquifer, and the porosity, ϕ, rock density, ρ_r, and groundwater density, ρ_w, are assumed to be constant with depth. When the minimum principal total stress is horizontal, we approximate it using Poisson's ratio, ν (Zoback, 2007, p.281):

$$p_{\text{frac}} = \frac{\nu}{1-\nu}\left((1-\phi)\rho_r g D + \phi \rho_w g D\right). \tag{6}$$

To estimate the direction of the minimum principal stress, we use a nationwide map of stress in the United States (Zoback and Zoback, 1980).

We use a simple model to determine how much CO_2 can be injected before the aquifer pressure reaches the fracture pressure. While there are many models of CO_2 injection (e.g.,(Mathias et al., 2009; Birkholzer et al., 2009)), we develop a model for our ideal system so that the pressure-limited and migration-limited capacities can be compared (Fig. 1). In addition to assumptions in this system discussed previously, we assume:

1. Zero lateral strain and constant vertical stress (Wang, 2000).
2. Pressure boundaries are far enough away that they do not affect the pressure at the well array.
3. The compressibility of CO_2 at aquifer conditions is equal to the compressibility of the aquifer brine.
4. The geomechanical effects of multiphase flow are negligible.

The assumptions of zero lateral strain and constant vertical stress in the aquifer allows the flow and poromechanics to be decoupled, reducing the model to a diffusion problem (Fig. 3) (Wang, 2000). Assuming that the compressibility of CO_2 is equal to the compressibility of water results in an overestimation of the pressure rise during injection since water has a lower compressibility than CO_2, but will likely provide results that are sufficiently accurate for this study.

In our model system (Fig. 3), the evolution of pressure as a function of the lateral coordinate, x, and the injection time, t, is governed by (Pinder and Gray, 2008):

$$c\partial_t p - \frac{k}{\mu_w}\partial_{xx} p = \delta(x)\frac{Q}{HW}, \qquad -\infty < x < \infty, \quad t > 0, \tag{7}$$

where c is the bulk compressibility, k is the intrinsic permeability, μ_w is the brine viscosity, and Q is the volume injection rate (Fig. 3). The conditions at infinity are:

$$p|_{x\to\pm\infty} \to 0, \quad \partial_x p|_{x\to\pm\infty} \to 0, \qquad t > 0. \tag{8}$$

Assuming that the pore pressure is initially hydrostatic, the initial condition is:

$$p(x, t=0) = \rho_w g D, \qquad -\infty < x < \infty. \tag{9}$$

This equation admits a similarity solution in the variable $x/\sqrt{t}$ (Mattheij et al., 2005, Ch.10):

$$p(x,t) = \rho_w g D + \frac{Q}{HWc\kappa}\left[\sqrt{\frac{\kappa t}{\pi}}\exp\left(\frac{-x^2}{4\kappa t}\right) - \frac{1}{2}|x|\operatorname{erfc}\left(\frac{|x|}{\sqrt{4\kappa t}}\right)\right], \tag{10}$$

where $\kappa = k/(\mu_w c)$. The maximum pressure occurs at the well array:

$$p_{\text{well}}(t) = \rho_w g D + \frac{Q}{HWc}\sqrt{\frac{t}{\pi\kappa}}. \tag{11}$$

While this equation is based on continuous injection, it correctly predicts the maximum pressure if injection stops at time T, since the pressure drops immediately after injection stops.

We use the equation for pressure at the well array to derive an expression for the pressure-limited storage capacity. We set the well pressure at the end of injection, $p_{\text{well}}(T)$, to be equal to the

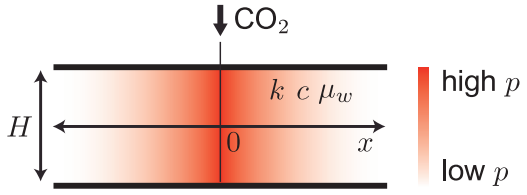

Fig. 3. To calculate pressure-limited capacity, we model how the pressure in an aquifer rises due to injection. Since we assume that the aquifer is homogeneous and anisotropic, and since we neglect multiphase flow effects, the pressure rise (red) is uniform along the thickness of the aquifer, H, and the model is one-dimensional in the lateral direction. The key parameters are the permeability, k, the compressibility, c, and the brine viscosity, μ_w. With the pressure model, we calculate how much CO_2 can be injected before the pressure rise at the well array exceeds the fracture pressure. (For interpretation of the references to color in this figure legend, the reader is referred to the web version of this article.)

fracture pressure, p_{frac}, and solve for the injection rate, Q. Since the total volume injected at time T is QT, the storage capacity is $\rho_g QT$:

$$C_p = \rho_g HW \sqrt{\frac{\pi kc}{\mu_w}} (p_{frac} - \rho_w gD) T^{1/2}. \quad (12)$$

This equation shows that the pressure-limited capacity grows as the square root of the injection time. While it was derived assuming a constant injection rate, the same scaling occurs if we adopt a ramp-up/ramp-down injection scenario, in which the injection rate first increases linearly with time up to time $T/2$ and then decreases linearly to zero at time T (Szulczewski, 2009).

4. Comparison of pressure and migration constraints

The more limiting constraint leads to the smaller capacity. As a result, we compare the relative severity of the constraints by comparing the capacities (Eqs. (3) and (12)):

$$\frac{C_m}{C_p} = \frac{L\phi S_{gr}\varepsilon}{(p_{frac} - \rho_w gD)} \sqrt{\frac{\mu_w}{\pi kcT}}. \quad (13)$$

When $C_m/C_p > 1$, the pressure-limited capacity is smaller so pressure constraints are more important than migration constraints. This tends to occur when the aquifer is shallow and long, the permeability is low but the porosity is high, and the injection time is short. It also tends to occur when the viscosities of the CO_2 and brine are more similar since the storage efficiency factor, ε, is inversely proportional to the mobility ratio, M.

When $C_m/C_p < 1$, the migration-limited capacity is smaller and migration constraints are more important. This tends to occur when the aquifer is deep but not very long, the permeability is high but the porosity is low, the injection time is long, and the fluid viscosities are very dissimilar.

Since the pressure-limited capacity increases with the duration of the injection period, $C_p \sim \sqrt{T}$, while the migration-limited capacity, C_m, is independent of time, there is generally a crossover from pressure-limited to migration-limited capacity as a function of injection duration. Equating the expressions for pressure-limited and migration-limited capacities yields a formula for the crossover time, T_c:

$$T_c = \frac{\mu_w}{\pi kc} \left(\frac{L\phi S_{gr}\varepsilon}{p_{frac} - \rho_w gD} \right)^2. \quad (14)$$

5. Pressure and migration constraints in the Fox Hills Sandstone

We demonstrate the competition between pressure and migration constraints in the Fox Hills Sandstone. This reservoir lies in the Powder River Basin in Wyoming and Montana (Fig. 4). It consists of continuous marine and non-marine sandstones with siltstone and minor shale (Whitehead, 1996). The relevant geohydrologic data for the reservoir are listed in Table 1.

The top boundary of the Fox Hills Sandstone is an extensive caprock called the Upper Hell Creek Confining Layer (Hovorka et al., 2003). It consists of lower-coastal-plain muddy sandstones. The bottom boundary is an aquiclude composed of marine shale and siltstone (Whitehead, 1996, Fig. 50). We identify lateral boundaries at major faults, outcrops, places where the caprock contains more than 50% sand, and places shallower than 800 m (Fig. 5A).

To determine how to orient the injection well array, we identify the dominant direction in which CO_2 would migrate in the aquifer. We use an expression derived in (MacMinn et al., 2010) to evaluate

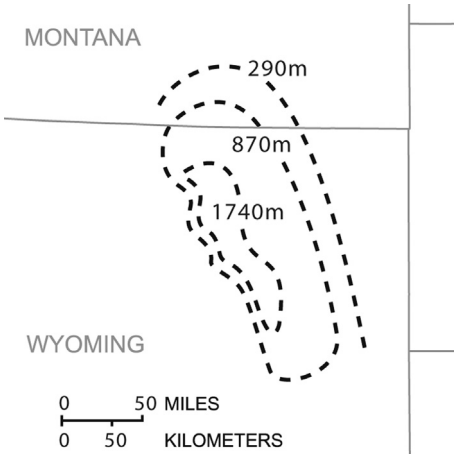

Fig. 4. We illustrate how both pressure and migration can constrain storage capacity in the Fox Hills Sandstone, an aquifer in Montana and Wyoming identified as a potential CO_2 storage reservoir. The depth contours show that the aquifer is asymmetric, with a gently sloping eastern margin and a steeply dipping western margin (Hovorka et al., 2003).

the relative strength of migration due to groundwater flow and slope:

$$\frac{N_s}{N_f} = \frac{(\rho_w - \rho_g) g k k_{rg}^* \sin\theta}{U\mu_g}, \quad (15)$$

where N_s is the strength of upslope migration, N_f is the strength of groundwater flow, θ is the aquifer slope, and U is the Darcy velocity of the groundwater. In the Fox Hills Sandstone, this ratio is about 20, indicating that the dominant migration direction is upslope. As a result, we orient the injection well array parallel to the aquifer's depth contours (Fig. 4).

With the well array in this orientation, we set the length of the aquifer, L, to the distance between the two lateral fault boundaries. Substituting the aquifer length and the data from Table 1 into Eq. (3), we calculate the migration-limited capacity to be about 3 metric gigatons of CO_2 ($GtCO_2$). We draw the areal extent of the trapped CO_2 and the corresponding well array in Fig. 5B.

We calculate the pressure-limited capacity with Eq. (12) and data from Table 1. Comparing this capacity to the migration-limited

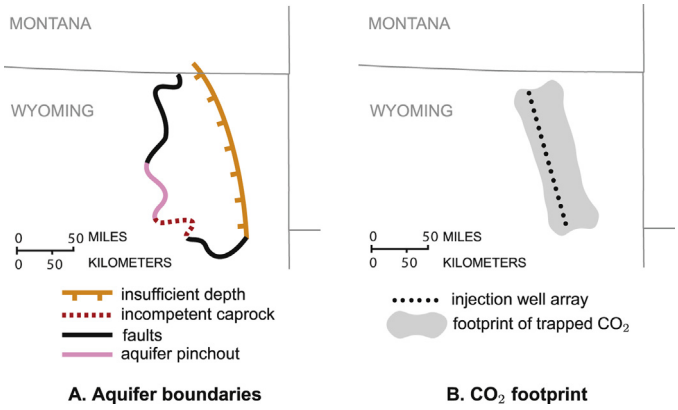

Fig. 5. (A) We set the eastern boundary of the Fox Hills Sandstone where the top of the aquifer becomes shallower than 800 m (Hovorka et al., 2003), the approximate depth at which CO_2 changes from a supercritical fluid to a gas. We use this boundary to ensure that CO_2 is stored efficiently in a high-density state. We set the remaining boundaries at large faults (Whitehead, 1996, Fig. 56), places where the caprock has more than 50% s and (Hovorka et al., 2003), and places where we interpret the reservoir to pinchout (Whitehead, 1996, Fig. 56). (B) The footprint of residually-trapped CO_2 fills a large region of the aquifer within the established boundaries, extending updip from the well array.

Table 1
Parameters for the Fox Hills Sandstone.

Parameter	Symbol	Value	Data Source	Reference
Residual CO_2 saturation	S_{gr}	0.3	Estimated	Bennion and Bachu (2008) and Oak et al. (1990)
Connate water saturation	S_{wc}	0.4	Estimated	Bennion and Bachu (2008) and Oak et al. (1990)
Endpoint relative permeability to CO_2	k^*_{rg}	0.6	Estimated	Bennion and Bachu (2008) and Oak et al. (1990)
Compressibility (GPa^{-1})	c	0.1	Estimated	Wang (2000, Table C1)
Undrained Poisson ratio	ν	0.3	Estimated	Wang (2000, Table C1)
Geothermal gradient (°C/km)	G_T	30	Aquifer data	Nathenson and Guffanti (1988)
Surface temperature (°C)	T_s	10	Aquifer data	National Climate Data Center (2010)
Depth to top of aquifer (m)	D	1000	Aquifer data	Hovorka et al. (2003, Map c1foxhillsg)
Net aquifer thickness (m)	H	200	Aquifer data	Hovorka et al. (2003, Map 4foxhills)
Length of model domain (km)	L	100	Aquifer data	Fig. 5
Width of well array (km)	W	200	Aquifer data	Fig. 5
Porosity	ϕ	0.2	Estimated	Freeze and Cherry (1979)
Caprock slope (degrees)	θ	1	Calculated	Hovorka et al. (2003, Map c1foxhillsg)
Darcy velocity (cm/year)	U	10[a]	Calculated	Whitehead (1996, Fig.56), McPherson and Cole (2000)
Intrinsic permeability (mD)	k	100	Calculated	McPherson and Cole (2000)
Brine density (kg/m^3)	ρ_w	1000	Calculated	Batzle and Wang (1992)
CO_2 density (kg/m^3)	ρ_g	500	Calculated	CCS Technologies at MIT (2011)
Brine viscosity (mPa s)	μ_w	0.7	Calculated	Batzle and Wang (1992)
CO_2 viscosity (mPa s)	μ_g	0.04	Calculated	CCS Technologies at MIT (2011)
Fracture pressure (MPa)	p_{frac}	10	Calculated	Eq. (6); (Zoback and Zoback, 1980)

[a] We calculate the Darcy velocity using Darcy's law with a head gradient of 0.003 (Whitehead, 1996, Fig. 56).

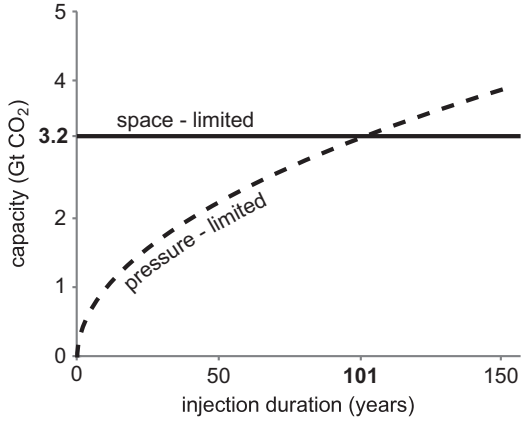

Fig. 6. The pressure-limited capacity grows with the square root of injection time (dashed curve) [Eq. (12)], but the migration-limited capacity is constant (solid curve). In the Fox Hills Sandstone, the capacity curves cross at an injection time of about 100 years, indicating that pressure constraints are more limiting for injection times less than 100 years, but migration constraints are more limiting for longer times.

capacity shows that, since the pressure-limited capacity grows as $T^{1/2}$, it is smaller than the migration-limited capacity for short injection periods. However, it eventually becomes larger than the migration-limited capacity at long injection periods, as shown in Fig. 6. This indicates that pressure constraints are more limiting for short injection periods, while migration constraints become more limiting for long injection periods.

Acknowledgments

Funding for this work was provided by the US Department of Energy under grant DE-FE0002041, the MIT Energy Initiative, the Reed Research Fund, the Martin Family Society of Fellows for Sustainability, and the ARCO Chair in Energy Studies.

References

Bachu, S., Bonijoly, D., Bradshaw, J., Burruss, R., Holloway, S., Christensen, N.P., Mathiassen, O.M., 2007. CO_2 storage capacity estimation: methodology and gaps. Int. J. Greenh. Gas Control 1, 430–443.

Batzle, M., Wang, Z., 1992. Seismic properties of pore fluids. Geophysics 57, 1396–1408.

Bear, J., 1972. Dynamics of Fluids in Porous Media. Elsevier, New York.

Bennion, D.B., Bachu, S., 2008. Drainage and imbibition relative permeability relationships for supercritical CO_2/brine and H_2S/brine systems in intergranular sandstone, carbonate, shale, and anhydrite rocks. Soc. Petrol. Eng. J. 11, 487–496.

Birkholzer, J.T., Zhou, Q., Tsang, C., 2009. Large-scale impact of CO_2 storage in deep saline aquifers: A sensitivity study on pressure response in stratified systems. Int. J. Greenh. Gas Control 3, 181–194.

Bradshaw, J., Bachu, S., Bonijoly, D., Burruss, R., Holloway, S., Christensen, N.P., Mathiassen, O.M., 2007. CO_2 storage capacity estimation: issues and development of standards. Int. J. Greenh. Gas Control 1, 62–68.

Cappa, F., Rutqvist, J., 2011a. Impact of CO_2 geological sequestration on the nucleation of earthquakes. Geophys. Res. Lett. 38, L17313.

Cappa, F., Rutqvist, J., 2011b. Modeling of coupled deformation and permeability evolution during fault reactivation induced by deep underground injection of CO_2. Int. J. Greenh. Gas Control 5, 336–346.

CCS Technologies at MIT. CO_2 thermophysical property calculator. http://sequestration.mit.edu/tools/index.html (Accessed April 2011).

Dooley, J.J., 2011. Valuing national and basin level geologic CO_2 storage capacity assessments in a broader context. Int. J. Greenh. Gas Control 5, 177–178.

Dooley, J.J., Dahowski, R.T., Davidson, C.L., Bachu, S., Gupta, N., Gale, J., 2004. A CO_2 storage supply curve for North America and its implications for the deployment of carbon dioxide capture and storage systems. In: Proceedings of 7th International Conference on Greenhouse Gas Control Technologies, vol. 1, Peer-reviewed papers and plenary presentations.

Ehlig-Economides, C., Economides, M.J., 2010. Sequestering carbon dioxide in a closed underground volume. J. Petrol. Sci. Eng. 70, 118–125.

Freeze, R.A., Cherry, J.A., 1979. Groundwater. Prentice Hall, Upper Saddle River, NJ, USA.

Gasda, S.E., Nordbotten, J.M., Celia, M.A., 2011. Vertically-averaged approaches for CO_2 migration with solubility trapping. Water Resour. Res. 47, W05528.

Hesse, M.A., Orr Jr., F.M., Tchelepi, H.A., 2008. Gravity currents with residual trapping. J. Fluid Mech. 611, 35–60.

Hovorka, S.D., Romero, M.L., Warne, A.G., Ambrose, W.A., Tremblay, T.A., Trevino, R.H., Sasson, D., 2003. Brine-Formation Database. http://www.beg.utexas.edu/environqlty/co2seq/dispslsalnt01.htm

IPCC, 2005. In: Metz, B., et al. (Eds.), Special Report on Carbon Dioxide Capture and Storage. Cambridge University Press, Cambridge, UK/New York, NY, USA.

Juanes, R., MacMinn, C.W., Szulczewski, M.L., 2010. The footprint of the CO_2 plume during carbon dioxide storage in saline aquifers: storage efficiency for capillary trapping at the basin scale. Transp. Porous Media 82, 19–30.

Juanes, R., Spiteri, E.J., Orr Jr., F.M., Blunt, M.J., 2006. Impact of relative permeability hysteresis on geological CO_2 storage. Water Resour. Res. 42, W12418.

Lackner, K.S., 2003. A guide to CO_2 sequestration. Science 300, 1677–1678.

MacMinn, C.W., Szulczewski, M.L., Juanes, R., 2010. CO_2 migration in saline aquifers. Part 1. Capillary trapping under slope and groundwater flow. J. Fluid Mech. 662, 329–351.

MacMinn, C.W., Szulczewski, M.L., Juanes, R., 2011. CO_2 migration in saline aquifers. Part 2. Combined capillary and solubility trapping. J. Fluid Mech. 688, 321–351.

Mathias, S.A., Hardisty, P.E., Trudell, M.R., Zimmerman, R.W., 2009. Screening and selection of sites for CO_2 sequestration based on pressure buildup. Int. J. Greenh. Gas Control 3, 577–585.

Mattheij, R.M.M., Rienstra, S.W., ten Thije Boonkkamp, J.H.M., 2005. Partial Differential Equations: Modeling, Analysis, Computation. SIAM, Philadelphia, USA.

McPherson, B.J.O.L., Cole, B.S., 2000. Multiphase CO_2 flow, transport and sequestration in the Powder River Basin, Wyoming, USA. J. Geochem. Explor. 69-70, 65–69.

MIT, 2007. The Future of Coal - An Interdisciplinary MIT Study. MIT Press, Cambridge, MA, USA.

Morris, J.P., Hao, Y., Foxall, W., McNab, W., 2011. A study of injection-induced mechanical deformation at the In Salah CO_2 storage project. Int. J. Greenh. Gas Control 5, 270–280.

Nathenson, M., Guffanti, M., 1988. Geothermal gradients in the conterminous United States. J. Geophys. Res. 93, 6437–6450.

National Climate Data Center, 2010. Mean Daily Average Temperature Map of the United States. http://cdo.ncdc.noaa.gov/cgi-bin/climaps/climaps.pl

National Energy Technology Laboratory, 2010. Carbon Sequestration Atlas of the United States and Canada, 3rd ed. http://www.netl.doe.gov/technologies/carbon_seq/refshelf/atlasIII/index.html

Nicot, J.P., 2008. Evaluation of large-scale CO_2 storage on fresh-water sections of aquifers: An example from the Texas Gulf Coast Basin. Int. J. Greenh. Gas Control 2, 582–593.

Oak, M.J., Baker, L.E., Thomas, D.C., 1990. Three-phase relative permeability of Berea sandstone. J. Pet. Technol. 42, 1054–1061.

Orr Jr., F.M., 2009. Onshore geologic storage of CO_2. Science 325, 1656–1658.

Pinder, G.F., Gray, W.G., 2008. Essentials of Multiphase Flow and Transport in Porous Media. John Wiley and Sons, Hoboken, New Jersey.

Rogelj, J., McCollum, D.L., Reisinger, A., Meinshausen, M., Riahi, K., 2013. Probabilistic cost estimates for climate change mitigation. Nature 493, 79–83.

Scott, V., Gilfillan, S., Markusson, N., Chalmers, H., Haszeldine, R.S., 2013. Last chance for carbon capture and storage. Nat. Clim. Chang. 3, 105–111.

Szulczewski, M.L., 2009. Storage capacity and Injection Rate Estimates for CO_2 Sequestration in Deep Saline Aquifers in the Conterminous United States. Massachusetts Institute of Technology, Master's thesis.

Szulczewski, M.L., MacMinn, C.W., Herzog, H.J., Juanes, R., 2012. Lifetime of carbon capture and storage as a climate-change mitigation technology. Proc. Natl. Acad. Sci. U. S. A. 109, 5185–5189.

Wang, H.F., 2000. Theory of Linear Poroelasticity. Princeton University Press, Princeton, NJ, USA.

Whitehead, R.L., 1996. The Ground Water Atlas of the United States, Montana, North Dakota, South Dakota, Wyoming. http://capp.water.usgs.gov/gwa/ch_i/index.html

Yortsos, Y.C., 1995. A theoretical analysis of vertical flow equilibrium. Transp. Porous Media 18, 107–129.

Zhou, Q., Birkholzer, J.T., Tsang, C., Rutqvist, J., 2008. A method for quick assessment of CO_2 storage capacity in closed and semi-closed saline formations. Int. J. Greenh. Gas Control 2, 626–639.

Zoback, M.D., 2007. Reservoir Geomechanics. Cambridge University Press, New York, NY, USA.

Zoback, M.L., Zoback, M., 1980. State of stress in the conterminous United States. J. Geophys. Res. 85, 6113–6156.